Simulation and Analysis of Flight Altitude and Images Overlaps Impact on 3D Reconstruction Accuracy in UAV Photogrammetry

Mohammad Saadatseresht [1], Ali Erfanzadeh [2], Saeid Homayouni [3]*

[1] *Associate Professor of Photogrammetry, School of Surveying and Geospatial Engineering, College of Engineering, University of Tehran, Iran*

[2] *Master student of photogrammetry, School of Surveying and Geospatial Engineering, College of Engineering, University of Tehran, Iran*

[3] *Associate Professor of Environmental Remote Sensing and Geomatics, Center for Water, Earth, and Environment, Institut national de la recherche scientifique, Quebec, Canada*

ABSTRACT

Flight altitude and image overlap are critical factors affecting the accuracy of 3D reconstruction in UAV photogrammetry. Understanding their behavior and impact on reconstruction accuracy is of utmost importance. However, conducting a comprehensive analysis of these parameters under operational conditions is both time-consuming and expensive. To address this challenge, we present a Monte Carlo Simulation (MCS) approach in this paper. We analyze the 3D reconstruction of a hypothetical point with known 3D coordinates, considering different levels of overlap and flight altitudes. Our simulation takes into account various sources of uncertainty and instability in the entire reconstruction process, including UAV exterior orientation parameter (EOP) instability, visibility issues, camera interior orientation parameter (IOP) instability, image observation noise, and aerial triangulation EOP noises. Through extensive experimental tests, we examine approximately 900,1610 cases to characterize the accuracy of a UAV photogrammetry system for mapping missions. This analysis yields several valuable guidelines. For instance, to achieve high accuracy in 3D reconstruction, we recommend increasing the coverage difference when the sum of overlap and sidelap exceeds 120%, and decreasing it when it falls below 120%. Furthermore, if the flight height increases by 20%, a corresponding 10% increase in total overlap and sidelap is recommended to compensate for the decrease in 3D reconstruction accuracy. The findings of this study can assist geomatics engineers and surveyors in effectively planning and designing UAV flight missions for mapping and monitoring projects.

1. Introduction

The use of drones for photogrammetry was initially reported in 1979 (*Cryderman et al., 2014*). However, significant advancements in both hardware and software for UAV photogrammetry systems have occurred in recent years. These advancements have led to improved quality, faster processing times, reduced costs, and a wide range of outputs, making UAV photogrammetry a highly effective system for collecting spatial data (*Kim et al., 2000; Senkal et al., 2021; Henri, 2009*).

UAV photogrammetry has emerged as one of the most effective methods for surveying positional data due to various factors, including time efficiency, cost-effectiveness, output diversity, and quality (*Erfanzadeh & Saadatseresht, 2021*). Several parameters influence the quality of UAV photogrammetry products (*Erfanzadeh & Saadatseresht, 2021*). Among these, flight altitude and image overlap are crucial parameters that directly impact the quality of 3D reconstruction and operational costs in the field (*Erfanzadeh & Saadatseresht, 2021*). To achieve optimal quality in UAV photogrammetry, a comprehensive

understanding of the behavior and impact of these parameters under different environmental and topographic conditions is essential (Erfanzadeh & saadatseresht, 2021).

In pursuit of this knowledge, researchers have experimented with different cameras, flight altitudes, and imaging overlaps to gather data using a trial and error approach. While this method considers various influential factors, it does not provide a comprehensive analysis of the impact of flight altitude and image overlap/sidelap on 3D reconstruction due to its associated costs and time requirements. As a result, users often have questions and uncertainties regarding this method. For instance, when considering safety concerns and increasing the flight altitude, how much should the overlaps be increased to achieve mapping accuracy? What is the relationship between flight altitude, image overlap/sidelap, and 3D reconstruction accuracy?

The design of a UAV photogrammetric network relies on various factors, including the desired image and geometrical quality, available financial resources, project objectives, technical facilities, environmental conditions, and safety constraints (Henri, 2009). In addition to sensor imaging properties, flight altitude, image overlap, and sidelap are crucial parameters in network design (Remondino et al., 2012). These parameters directly impact the quality of 3D reconstruction and operational costs in UAV photogrammetry (Radoslaw, 2017). To achieve optimal quality and accuracy in photogrammetric products, it is imperative to thoroughly study and model the behavior and impact of these parameters under different environmental and topographic conditions (Erfanzadeh & saadatseresht, 2021). In pursuit of this goal, researchers have collected UAV data using various cameras, flight altitudes, and image overlaps through trial and error and personal experiences (Radoslaw Jan, 2017). While these approaches consider important factors, a comprehensive analysis of the effects of flight altitude and image overlaps on 3D reconstruction is lacking due to the time and cost associated with such investigations. Previous studies have analyzed limited practical samples under different environmental conditions using default parameter values (Mesas-Carrascosa et al., 2017; Mesas-Carrascosa et al., 2015; Mesas-Carrascosa et al., 2016; Shahbazi et al., 2015; Radoslaw Jan, 2017; Zhang et al., 2011). However, these studies do not provide a comprehensive and reliable analysis of the problem at hand.

Studies show that by increasing the overlap and sidelap, the Root Mean Square Error (RMSE) value of the control points will decrease, while for the checkpoints, it shows a random behavior (Radoslaw Jan, 2017). Generally, the 3D reconstruction precision will increase by increasing the image overlap, but its impact is less than the flight altitude

(Senkal et al., 2021). The horizontal error with a slope of 0.03 will increase the flight height. In addition, the 3D reconstruction precision will increase by increasing the overlap, which is considerable in low-flight altitudes (Mesas-Carrascosa et al., 2016). The increment of flight altitude will not always lead to higher values of RMSE, and the increment of overlap will improve the precision, strength, and reliability of results (Mesas-Carrascosa et al., 2017).

Several studies have revealed important findings regarding the impact of overlap and sidelap on 3D reconstruction accuracy. Radoslaw Jan (2017) demonstrated that increasing the overlap and sidelap results in a decrease in the Root Mean Square Error (RMSE) of control points. However, the behavior of checkpoints appears to be more random in response to these changes. Generally, increasing the image overlap contributes to improved precision in 3D reconstruction, although its effect is less significant compared to flight altitude (Senkal et al., 2021). It has been observed that increasing the flight altitude can lead to a gradual increase in horizontal error with a slope of 0.03. On the other hand, increasing the overlap is particularly impactful in achieving higher 3D reconstruction precision, especially at lower flight altitudes (Mesas-Carrascosa et al., 2016). Importantly, it should be noted that elevating the flight altitude does not always result in higher RMSE values, while increasing the overlap can enhance precision, robustness, and result reliability (Mesas-Carrascosa et al., 2017).

While several studies have examined the relationship between flight altitude and image overlap, most of these investigations have focused on specific cases and limitations (Cryderman et al., 2014; Senkal et al., 2021; Rock et al., 2012; Mesas-Carrascosa et al., 2017; Mesas-Carrascosa et al., 2015; Mesas-Carrascosa et al., 2016; Shahbazi et al., 2015; Radoslaw Jan, 2017; Zhang et al., 2011). However, these studies are not comprehensive and do not provide an in-depth analysis of the impact of flight altitude and image overlap on 3D reconstruction accuracy.

In this study, a simulation-based approach was employed to comprehensively analyze the behavior and impact of flight altitude, image overlap, and sidelap on the quality of 3D reconstruction. The simulation method was chosen due to its cost-effectiveness and flexibility. It allows for a thorough assessment of different UAV configurations under various conditions by adjusting camera parameters and error parameters. This approach offers significant advantages in evaluating the accuracy of 3D reconstruction in UAV

photogrammetry while maintaining a high level of flexibility and minimizing costs.

In order to comprehensively analyze the impact of flight altitude and image overlap on 3D reconstruction accuracy, a series of simulation analyses were conducted. The simulation focused on a hypothetical ground point with known absolute coordinates. It was assumed that the point was located on a non-textured, non-specular, and stationary surface, allowing for effective multi-view image matching.

The simulation involved capturing images at different altitudes and overlaps, followed by the calculation of the 3D coordinates of the imaged point using the space intersection method. To simulate the inherent random errors and instabilities present in real-world scenarios, Gaussian distribution functions were applied to introduce variations in the parameters. To ensure the reliability and comprehensive analysis of the results across different environmental conditions, the tests were performed in five modes: Ideal, Excellent, Good, Moderate, and Poor.

The Monte Carlo Simulation (MCS) method was employed to investigate the quality of 3D reconstruction for the ground point. This method allowed for a thorough examination of the reconstruction accuracy and provided detailed insights into the impact of flight altitude and image overlap. Further details regarding the analysis and its findings will be presented in subsequent sections.

It is important to acknowledge that this research is a simulation-based study and has certain limitations. To simplify the research and avoid additional complexities, the study focused on ten network design parameters listed in Table 2, considering five states. Consequently, certain real-world factors and situations were not incorporated into the simulation. One such example is the influence of flight speed and the need to strike a balance between sensor firing speed limitations due to hardware constraints and image blurring.

In practice, increasing the forward overlap would require faster image firing, which could result in the UAV needing to fly at very slow speeds (< 3 m/s). However, this may not be economical due to increased flying times and limitations imposed by battery life. Therefore, the present study does not address questions such as whether reducing side overlap would actually decrease overall flight times when the image-firing system cannot keep up. Additionally, the potential impact of increasing shutter speed or dealing with blurry images on precision is not explored if the image firing system can handle a higher forward overlap.

These important questions and situations will be addressed in future research, where a more comprehensive analysis can be conducted, taking into account the various factors and constraints associated with flight speed, image-firing capabilities, and image quality.

2. 3D Reconstruction Simulation

In order to study the complex behavior of UAV photogrammetry, our research plan involves implementing a simulation approach that progresses from simple to more complex cases. This will be done in three phases: (1) Analytical simulation of the 3D reconstruction of a hypothetical point. (2) Analytical simulation of the 3D reconstruction of a grid of hypothetical points. (3) Digital simulation of the 3D reconstruction of a hypothetical textured surface. The current paper focuses on phase (1) of the research, where we conduct an analytical simulation of the 3D reconstruction of a single hypothetical point. Out of the ten parameters considered in the analytical simulation, our emphasis is on two specific parameters: imaging sidelap/overlap and flying height.

To capture the concept of error propagation, we have utilized the Monte Carlo Simulation (MCS) method in our analytical 3D reconstruction simulation. This method enables us to simulate and analyze the impact of uncertainties and instabilities throughout the process of 3D reconstruction accurately.

Object Space Simulation
- Simulation of the parameters of camera exterior orientation in ideal mode
- Simulation of the parameters of camera exterior orientation parameters in real mode

Image Space Simulation
- Calculating the ideal image coordinates of the assumed point in each image
- Investigating the visibility of the assumed point in each image
- Simulation of the instability of interior orientation parameters

Systematic and Random Errors Simulation
- Applying the distortions caused by the instability of the camera to image coordinates
- Applying random noise to image observations
- Applying random noise to exterior orientation parameters

3D Reconstruction Simulation
- 3D reconstruction of the assumed point
- Estimating the 3D reconstruction quality

Experimental Tests and Results
- Tests of the investigation of 3D reconstruction quality
- Analysis of test results

Figure **1**. An overview of the **3**D reconstruction simulation in UAV photogrammetry based on the Monte-Carlo strategy.

The Monte Carlo Simulation (MCS) method is a computational algorithm that relies on repeated random sampling to explore and analyze a problem's entire solution space (Kim et al., 2000). It is particularly useful when precise solutions cannot be obtained using specific algorithms and when there is a high degree of uncertainty (DOUG, 2007).

MCS involves performing multiple iterations of computations using random numbers, a task well-suited for computer implementation (Palisade). This method has gained popularity due to its ability to handle significant input uncertainties and analyze phenomena characterized by random behavior, instability, and uncertainty (Doringer, 2018).

In our study, we employed the MCS method to analyze the propagation of errors, considering the random behavior, instability, and uncertainty associated with calibration parameters, image observation errors, aerial triangulation errors, and flight navigation parameters. By simulating numerous iterations and incorporating random variations in these parameters, we obtained a more comprehensive understanding of how uncertainties impact the accuracy of 3D reconstruction.

To simplify the problem and streamline calculations, our simulation focuses on a single given point. The camera is positioned at a specific flight altitude, and imaging is carried out with predetermined image overlap and sidelap values. Users have the flexibility to determine the number of random errors and instability levels in various interior and exterior orientation parameters, as well as image observations.

Using the simulated rays, a space intersection is performed in the 3D space to reconstruct the given point. This reconstruction process is repeated within the framework of the Monte Carlo Simulation (MCS), allowing for the calculation of reconstruction errors and Root Mean Square Error (RMSE) measures. Mean errors are calculated for different network design parameters.

To facilitate the MCS, it is necessary to define the distribution function for random parameter errors. However, in UAV photogrammetry, the statistical behavior of random parameters is not well-established. In light of this, we apply the Gaussian distribution function as the distribution model for random errors and instabilities, based on the central limit theorem in statistics. This choice allows us to conduct the necessary tests and analysis within the simulation.

The flowchart for 3D reconstruction simulation in UAV photogrammetry can be divided into five sections (see Figure 1). This study aims to analyze and monitor the flight altitude as well as the overlap and sidelap of images, with respect to the quality of 3D reconstruction. In the following sections, each component of Diagram 1 will be thoroughly explained.

2.1. Simulation of exterior orientation parameters in ideal mode

Consider a given 3D point with coordinates X = [0 0 0]. Assuming a drone with specific characteristics is flying and capturing vertical images above this point at a height of h0 in multiple strips, with a defined overlap px and sidelap py (0 < px, py < 1) along the XY axis. Consequently, the exterior orientation parameters (EOP) will be determined for each imaging station in the ideal mode (refer to Figure 2). The initial flight altitude (h0) is chosen to meet the ground sample distance (GSD) requirements for the desired map, following the standard guidelines. As per Iranian mapping standards, the GSD0 for 1:500, 1:1000, and 1:2000 scale maps is 4cm, 8cm, and 16cm, respectively. Hence, the flight altitude is calculated using Equation (1), where ps represents the sensor pixel size, and c0 denotes the initial principal distance. Additionally, the flight altitude can be adjusted using Equation (2) by modifying the coefficient of the flight altitude to a value within the range of 0.5 < kh < 2. In Equation (2), kh represents the coefficient of variation, and h0 corresponds to the flight height required for a GSD of 4 cm.

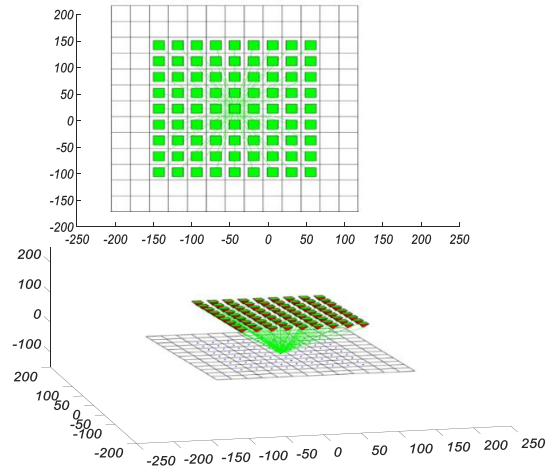$$h_0 = \frac{GSD_0 \cdot c_0}{h} \quad (1) \qquad\qquad h = k_h \cdot h_0 \quad (2)$$

Figure **2**. Simulation of the parameters of camera exterior orientation in the ideal mode

2.2. Simulation of exterior orientation parameters in real mode

In UAV photogrammetry, there exists a disparity in position and attitude between the exterior orientation parameters in real mode (EOP') and the ideal or design mode (EOP). This difference arises due to various factors such as the lightweight nature of the drone, the influence of

weather conditions, and navigation errors. To simulate the instability of the drone and its navigation, random errors with a specific standard deviation are introduced to the exterior orientation parameters of each image (refer to Figure 3).

According to Equation (3), the standard deviation of the position and attitude of the imaging stations is denoted as Sp and Sa, respectively. While it is possible to consider distinct standard deviations for position (XYZ) and attitude (ω, φ, κ or roll, pitch, yaw) along each of the three axes, doing so would complicate the simulation unnecessarily. Hence, to avoid this complexity, a uniform standard deviation is applied to both position and attitude parameters.

$$EOP' = EOP + dEOP$$

$$dEOP = [N(0, S_P) \, for \, xyz \, N(S_a) \, for \, roll, \, pitch, \, yaw] \quad (3)$$

where N (0, S) is a random value of the normal distribution function with the average 0 and the standard deviation S.
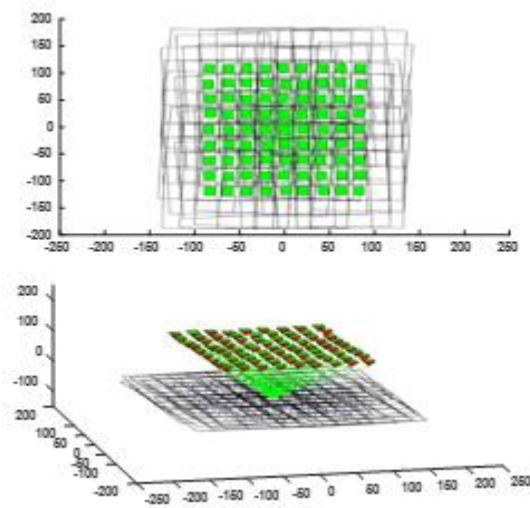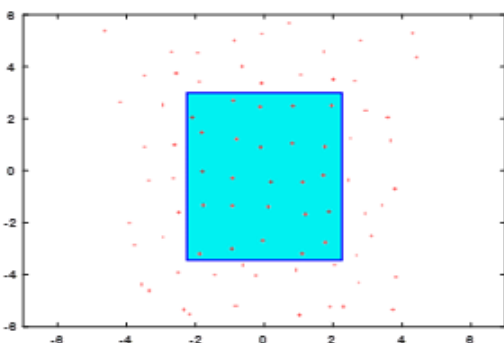

Figure 3. Simulation of the parameters of camera exterior orientation in real mode

2.3. Calculating ideal image coordinates of the given point in each image

Once the exterior orientation parameters of each image (EOPi') have been calculated, the 3D coordinates of the given point X = [0 0 0] in the coordinate system of each camera can be determined using equation (4). In this equation, Ti represents the coordinates of the image center, and Ri denotes the rotation matrix of the ith imaging station. Subsequently, by considering the collinearity

condition, the ideal image coordinates of the given point can be obtained using equation (5). In equation (5), c represents the principal distance of the camera lens (refer to Figure 4).

Figure 4. Calculating the ideal image coordinates of the given point in each image (mm)

$$X_i' = R_i'(X - T_i) = -R_iT' \quad X_i'\{X'_i, Y'_i, Z'_i\} \quad (4)$$

$$y_i = -c\frac{Y_i'}{z_i'} \quad and \quad x_i' = -c\frac{X_i'}{Z_i'} \quad (5)$$

2.4. Investigating the visibility of the given point in each image

If the image coordinates fall outside the range of the image, it indicates that the point is not visible, and as a result, the corresponding image should be excluded from the space intersection calculation. Therefore, for an image to be considered valid, it must satisfy two conditions outlined in Equation (6), ensuring that the image dimensions a and b (in pixels) align with the X-Y axes (as depicted in Figure 5). Equation (6) incorporates the pixel size of the camera, where b represents the height of the sensor, and a denotes its width.

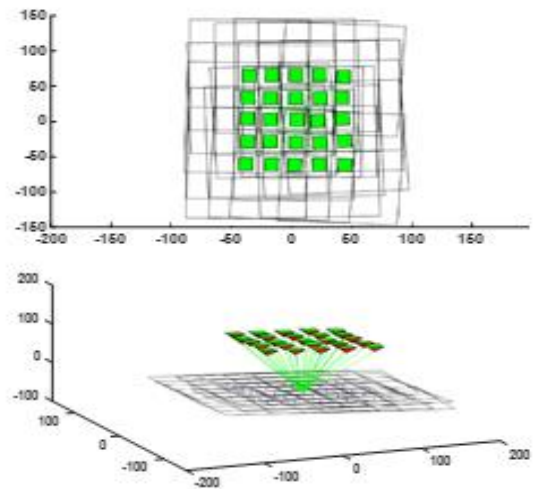$$|x_i| < \frac{ps.b}{2} \quad and \quad |y_i| < \frac{ps.a}{2} \quad (6)$$

Figure 5. Investigating the visibility of the given point in each image

2.5. Simulation of the interior orientation parameters of the non-metric and unstable camera

Let's suppose we have a digital camera with the principal distance of c0 and sensor dimensions of [a,b] (where a>=b) in pixels. The pixel size is ps micrometers, with a being aligned with the Y-axis and b aligned with the X-axis. Consequently, the ground sample distance (GSD) can be calculated using the formula GSD=ps.h/c, where h denotes the flight altitude.

In addition to the aforementioned parameters, the camera possesses interior orientation parameters (IOP) and other fixed parameters including c, x0, y0, radial lens distortion

coefficients *k1, k2, k3, k4,* lens dicentric distortion coefficients *P1, P2, P3, P4,* and affinity parameters *B1, B2,* which account for geometric image distortions. It is assumed that all of these parameters have random variations represented by *dIOP = N(0, SdIOP),* where *SdIOP* indicates the standard deviation of each parameter. The *dIOP* values reflect the instability of the non-metric camera and can lead to inaccuracies in applying the interior orientation parameters during 3D reconstruction.

It is important to note that while IOP and dIOP remain constant for all images, IOP remains the same while dIOP varies across different iterations of the Monte Carlo simulation (MCS). In order to simulate the values of IOP and dIOP, the calibration results of a camera can be utilized. For this study, the numerical calibration values of the Phantom 3 camera, obtained from a real operational project and with an image size of 3000x4000 pixels, are used and presented in Table 1.

Table 1. Calibration file of Phantom 4 camera

Calibration parameters	Unit	IOP calibration	IOP std dev	IOP real
C	mm	3.58910000	0.01620000	3.59491066
Xp	mm	-0.02420000	0.00060000	0.02411376
Yp	mm	0.01310000	0.00130000	0.01320203
K1	-	0.00163642	0.00005278	0.00162871
K2	-	-0.00005565	0.00000168	0.00005555
K3	-	-0.00000185	0.00000007	0.00000186
P1	-	-0.00001509	0.00000338	0.00001549
P2	-	-0.00025102	0.00000830	0.00025087
B1	-	-0.00000334	0.00000138	0.00000342
B2	-	0.00000000	0.00000041	0.00000006

In order to simulate the instability of the interior orientation parameters of the camera, the interior orientation parameters (IOP) and standard deviation of each one of them (S_{IOP}) are considered the calibration outputs of the camera of a real sample. Now, according to Gaussian distribution function $N(0, S_{dIOP})$, the changes of each parameter are calculated randomly, and image distortions *Δx, Δy* are calculated on an image grid with IOP and IOP'=IOP+dIOP. They are subtracted from each other so that the image remained distortion grid (*Δx, Δy*) that is equivalent to the non-metric camera instability- will be obtained by the Equation (7).

$$d\Delta x = d\Delta xIOP^{'} - d\Delta xIOP \quad , \quad d\Delta x = d\Delta yIOP^{'} - d\Delta yIOP \ (7)$$

Since in this simulation, we want to introduce T as the average image distortion caused by calibration error (per pixel) by the user, T is divided by the average value of the remaining distortion vectors *dΔx,dΔy:*

$$\frac{T}{\frac{\Sigma\sqrt{\Delta x^2 + \Delta y^2}}{m}}$$

Then, its value will be multiplied by the image distortion grid *dΔx, dΔy* so that the final image grid distortion average will equal T. In this expression, m is the number of the vertices of the above distortion grid.

2.6. Applying the distortions caused by the instability of the camera to image coordinates

As the distortion grid (*dΔx,dΔy*) of the camera's instability is obtained, the distortion of image observations will be calculated by bilinear interpolation and applied to image coordinates using Equation (8). It must be emphasized again that according to the iterative logic of the MCS method for the application of random search space for input variables aimed at the estimation of probable solution and also by considering the static mode of calibration parameters' distortions in each imaging station for simulation, in each iteration of MCS, the model of distortion is the same. However, in different iterations, it will change randomly (Figure 6).

$$x^{'} = x + d\Delta x \quad and \quad x^{'} = x + d\Delta x \qquad (8)$$
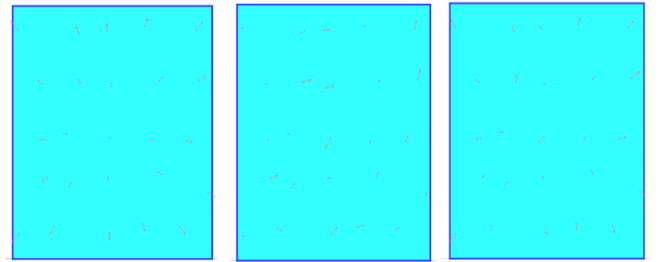

Figure 6. (a) the radial distortions caused by camera instability to image coordinates, (b) the random noise to image coordinates due to low image quality measurement, (c) the sum of these two types of image coordinates error

2.7. Applying random noise to image observations

In this stage, prior to the 3D reconstruction process, random errors of aerial triangulation parameters are considered, assuming a normal distribution function. Two standard deviations, SATa (angular) and SATp (positional), are defined as coefficients relative to the ground sample distance, based on real-world observations and expert knowledge (as shown in Table 2). These errors are then applied to the simulated exterior orientation parameters as noise, following Equation (10).

It is important to note that the nature of these random errors differs from the Sa and Sp errors associated with simulating instability in UAV navigation. In the second stage, these errors are applied to the observed rays visible in different images. These errors have an impact on the quality of ray intersection. In the process of space intersection, Sa and Sp errors alter the functional model of intersection equations based on the collinearity condition. On the other hand, sata and satp errors modify the statistical

model by incorporating a variance-covariance matrix of the exterior orientation elements.

As mentioned earlier, the user incorporates triangulation errors based on a coefficient of the ground sample distance (GSD). These errors can be calculated using equation (10), where kp represents the positional error coefficient and ka represents the rotational error coefficient of aerial triangulation relative to the GSD. In equation (10), Ka represents the coefficient of variation, h denotes the flight height, and GSD corresponds to the ground sampling distance, which is set at a size of 4cm.

$$s_{ATa} = \frac{K_a \cdot GSD}{h} \text{ and}$$

$$dEOP = [N(0, S_{ATp}) \, for X_o Y_o Z_o \, \& \, N(0, S_{ATa}) \, for \omega \varphi \kappa] \text{ and}$$

$$EOP'' = EOP' + dEOP \tag{10}$$

2.8. 3D reconstruction of the given point

Now, we have image observations x″y″ that are affected by both camera interior orientation instability and random errors, as well as the exterior orientation parameters EOP″ of different images, which include random errors and UAV instability. By performing the space intersection of corresponding rays under these conditions, we can obtain the 3D coordinates of the given ground point while minimizing the sum of the squares of image residuals. This is achieved by minimizing Equation (11) while satisfying the collinearity condition equations. In Equation (11), x″i represents the image coordinates, c denotes the principal distance of the camera (specifically, the Phantom 4 Pro in this case), R represents the components of the rotation matrix, and Ti denotes the positional parameters of the exterior orientation parameters.

$$F(X) = \sum \left(\left[x_i'' - \frac{c \cdot R_{1i} \cdot (X - T_i)}{R_{3i}(X - T_i)} \right]^2 + \left[y_i'' - \frac{c \cdot R_{2i} \cdot (X - T_i)}{R_{3i} \cdot (X - T_i)} \right]^2 \right)$$

$$(11)$$

2.9. Estimation of 3D reconstruction quality

The MCS method involves calculating possible solutions through iterations using different random values from the parameters' distribution function. In this study, the objective is to determine the relationship between overlap/sidelap, flight altitude, and the quality of 3D reconstruction. To achieve this, the 3D reconstruction is performed in different modes using n iterations of MCS, with n being set to 100. As a result, the reconstructed points X′ = [X′, Y′, Z′] are scattered around the given point X = [0 0 0].

Since the real value of the unknown and the number of iterations (n) are known, the estimated value for it, as well as the horizontal (RMSExy) and vertical (RMSEz) quality of the 3D reconstruction for the given point, can be estimated using the RSME (Root Mean Square Error) standard.

Thus far, we have discussed the proposed flowchart for 3D reconstruction in UAV photogrammetry. Moving forward,

the monitoring tests for flight altitude, longitudinal overlap, and sidelap of images will be conducted. The results obtained from these tests will be presented and analyzed in the following sections.

3. Experimental tests

In order to obtain more reliable results, it is necessary to conduct tests in various conditions that reflect different environmental and camera quality parameters. As mentioned earlier, the study considers five modes (Ideal, Excellent, Good, Moderate, and Poor) based on the experiences of the close-range photogrammetry laboratory at Tehran University (as shown in Table 2). These modes represent different values and errors for the parameters being tested, such as flight altitude and overlap/sidelap.

For each value of the specified parameter, imaging and reconstruction of the given ground point are performed using 100 iterations of the Monte Carlo Simulation (MCS) experiment, following the variation column in Table 2. Consequently, the ground point is reconstructed 100 times for each parameter value. The average horizontal and vertical errors in the 3D reconstruction are then estimated using the RMSE standard. The values in Table 2 represent the standard deviation of the Gaussian distribution functions that generate random values for the corresponding parameter in the MCS iterations. In complex systems, instead of propagating errors through statistical modeling of observation and parameter noise, the statistical behavior is analyzed using the trial and error method (DOUG, 2007).

It is important to note that when a parameter is expressed as a standard deviation, it represents the average values where 70% of the values are lower than the given value, and 30% are between this value and three times this value. Based on Table 2, Sa and Sp represent the standard deviations of tilt angle and position deviations, respectively, relative to the ideal or design conditions. Ka and kp are the coefficients of the ground sample distance (GSD) used to calculate the standard deviations of rotational and positional errors in aerial triangulation, which also affect the rotational and positional errors of image projection centers. T represents the mean image distortion caused by camera instability, while So indicates the standard deviation of image observations. Px and py represent the overlap and sidelap of images, respectively, and kc and kh are the coefficients of focal length and flight altitude, which have constant values (set to 1) across all five modes for the analysis of image overlaps.

Furthermore, the study examines the impact of UAV flight altitude on the accuracy of 3D reconstruction under specific cases of imaging overlaps. The focal length is determined based on Table 1, and the flight altitude value is set according to a 1/500 scale or a ground sample distance of 4cm.

The reason for using the Ideal and Poor modes can be understood by examining their parameter values in Table 2. In the Ideal mode, the UAV motion is perfectly stable, resulting in zero values for So, Sa, and Sp. Additionally, the camera geometry is highly stable, indicated by T = 0.025 pixels, which means that the camera's interior orientation

parameters vary within a range of 1:40 pixels for different images. The image quality is exceptionally high, with the image observation error having a standard deviation of So = 0.05 pixels, which is close to zero. Moreover, the aerial triangulation error for the exterior orientation parameters

of each image is characterized by rotational and positional errors of Ka and Kp within the range of 0.1 pixels, which is a typical range for professional metric cameras.

Table 2. *Values of parameters, standard deviation, and the range of their changes for five modes of Ideal, Excellent, Good, Moderate, and Poor according to the experience of the expert person that indicates different environmental conditions and camera quality.*

Parameter/Mode	Unit	Ideal	Excellent	Good	Moderate	Poor	Changes
S_a	degree	0	1	2	4	8	-
S_p	meter	0	0.2	0.5	1	5	-
T	pixel	0.025	0.1	0.2	0.5	1	-
S_o	pixel	0.05	0.2	0.4	1	2	-
k_a	GSD	0.1	0.2	0.5	1	2	-
k_p	GSD	0.1	0.2	0.5	1	2	-
p_x	%	90	80	80	80	60	30:5:95
p_y	%	80	80	70	60	60	30:5:95
k_c	-	1	1	1	1	1	-
k_h	-	1	1	1	1	1	0.5:0.075:2

These parameter values gradually increase from the Ideal to the Poor modes to represent different conditions related to the UAV, camera, and environment. The increasing values reflect varying levels of instability and lower quality in UAV motion, camera geometry, image observations, and aerial triangulation errors. By considering these different modes, the study aims to assess the impact of these factors on the 3D reconstruction process.

Suppose we need to assess the overlap and sidelap of an image. To accomplish this, we can simply choose a value from the "Changes" column in Table 2. Since the desired point is visible in at least two photos, it is not possible to have both overlap and sidelap less than 50%. Let's assume that the selected values for overlap and sidelap are 80% each. In order to simulate the 3D reconstruction process, we need to determine the camera type and its parameters. For this article, we utilize the parameters of the Phantom 4 Pro for the simulation. The next step involves introducing environmental conditions for imaging, which are determined based on the platform's tilt angle and shift, and then capturing the images. Following that, we simulate the application of camera distortion parameters to the photo observations, represented by parameter T in Table 2, whose value is the average distortion in the image. The third step in the simulation is applying the instability of the interior orientation parameters, denoted by the So parameter in Table 2. Once these parameters are applied, we proceed to simulate aerial triangulation errors for the purpose of the simulation and three-dimensional reconstruction. These errors are incorporated as two parameters: position and

rotation. Subsequently, the three-dimensional reconstruction is performed using the spatial intersection method and the least square error method. Let's assume that the 3D reconstruction process is proceeding ideally. Consequently, the aforementioned parameters are selected from the first column of Table 2. It is worth noting that, except for the instability calibration parameter, the mentioned parameters are applied to the observations using the standard deviation of the Gaussian distribution function. To account for the instability of the camera's interior orientation parameters, we simulate the error of the camera calibration parameters by considering the standard deviation of the Gaussian distribution function in the observation grid, which is obtained from the file of a real project.

3.1. Image overlap affecting 3D reconstruction quality

In order to assess the impact of image overlap and sidelap on the quality of 3D reconstruction, the extent of image overlaps and sidelap was increased by 5% from 30% to 95%, as indicated in the "change" column of Table 2. The Monte Carlo simulation (MCS) method was employed for each mode to replicate the imaging of ground points and their subsequent 3D reconstruction through 100 iterations. The first six parameters in Table 2 were subjected to a Gaussian noise model with predefined standard deviations. Given that the actual values of ground point coordinates and their corresponding 100 reconstructed positions using the MCS method were known, the quality of 3D reconstruction in each mode was evaluated using the root mean square error (RMSE) standard for horizontal (RMSExy), vertical

(RMSEz), and overall (RMSExyz) measurements. Furthermore, the relative changes in 3D reconstruction errors perpendicular to the flight strips were calculated using equation (12) to examine the variability of errors across different image overlaps.

$$\left(\frac{RMSEx - RMSEy}{RMSExy} \right) \tag{12}$$

This procedure is iterated across five modes: Ideal, Excellent, Good, Moderate, and Poor, corresponding to the adjusted standard deviations in Table 2. Consequently, a total of 90,000 tests are conducted by considering the five modes, 180 ordered pairs of overlap and sidelap, and 100 iterations of the Monte Carlo simulation (MCS). These tests are performed to analyze the impact of overlaps on 3D reconstruction, and their findings are summarized in Figure 8. It is important to note that if both overlap and sidelap are below 50%, it would be impossible to perform 3D reconstruction for all ground features, and therefore, these cases are disregarded.

Figure 7 depicts the minimum, mean, and maximum statistical parameters of horizontal and overall errors in 3D reconstruction, which are further visualized in Figure 8. In particular, diagrams (c) and (d) demonstrate that adjusting the image overlaps can significantly improve the horizontal error by up to 10 times and the overall 3D reconstruction error by up to five times (up to seven times in the ideal mode). Additionally, diagram (b) in Figure 7 illustrates that the mean error of 3D reconstruction (RMSExyz) in the Poor to Excellent modes is 23, 12, 6, and 2.5 times greater than the mean error in the ideal mode. This implies that environmental conditions and camera quality can amplify the overall 3D reconstruction error by more than 20 times.

In Figure 8, the horizontal and vertical axes represent the overlap and sidelap, respectively. With a 5% step length, the hypsographic charts display values for RMSEx, RMSEy, RMSEdxy (the relative heterogeneity of 3D reconstruction, i.e., absolute value of relative changes in horizontal errors based on Equation (12)), RMSExy as the horizontal error, RMSEz, and RMSExyz as the overall reconstruction error in the five modes. Several practical observations can be inferred from these results.

Firstly, the overlap values of px=95 and py=95 yield the lowest 3D reconstruction error (RMSExyz), while px=50 and py=30 exhibit the highest error. Furthermore, across the five modes, the maximum absolute difference in 3D reconstruction errors along the x and y directions ranges from 15% to 30% of the horizontal error, specifically in cases where overlap and sidelap are above 80% or below 55%. This indicates that a reduced number of intersected image rays weakens the network's effectiveness, leading to heterogeneity between x and y errors in 3D reconstruction. It is worth noting that higher image overlaps exponentially increase the number of rays and the intersection geometry is influenced by the overall airbases (i.e., the angle between the first and last rays) in both overlap and sidelap directions. Therefore, the overall base is dependent on the image dimensions, and considering the 3:4 ratio of the images in

this test (w=4000, h=3000 pixels), a 30% change will occur in the x error relative to y.

The diagrams in Figure 8 reveal that the 3D reconstruction error (RMSExyz) does not exhibit symmetrical behavior in the overlap/sidelap directions. On average, it is approximately 5% higher in the sidelap direction (based on numerical values not directly visible). This discrepancy arises because the longitudinal base for all overlapping images is smaller than the transversal base. Conversely, the horizontal error (RMSExy) of 3D reconstruction is approximately symmetrical and is not dependent on the overall base in both overlap and sidelap directions.
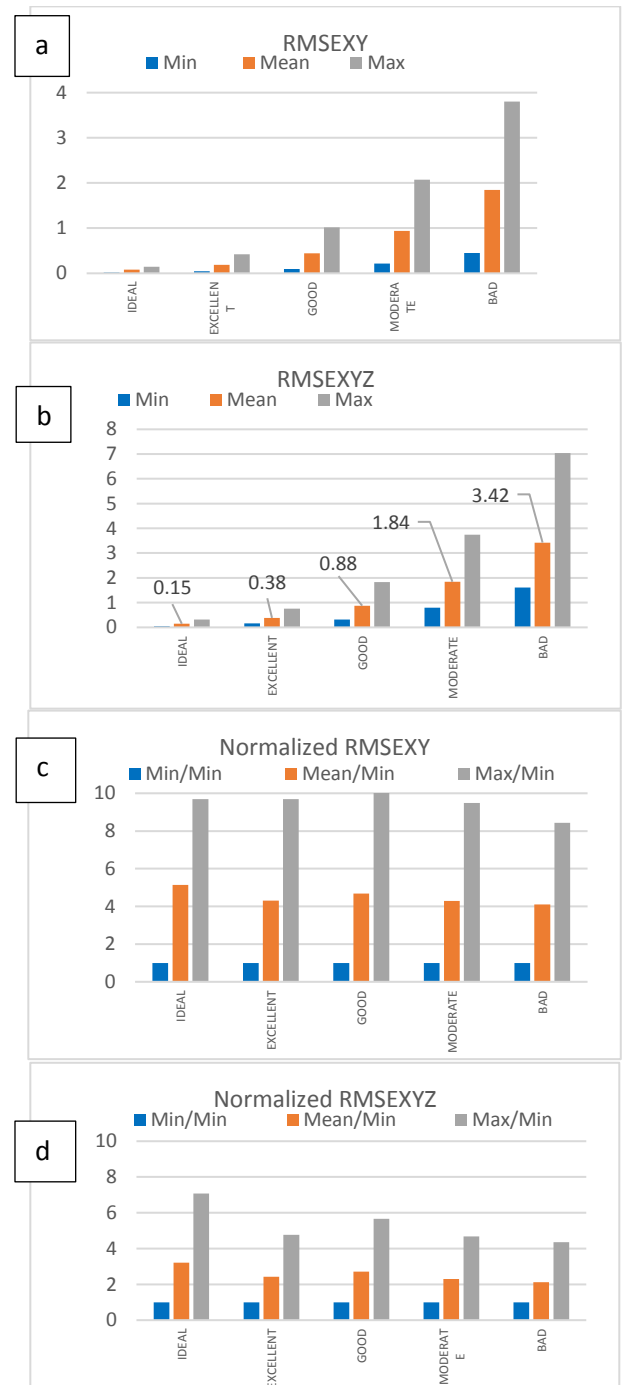

*Figure 7. Diagram of the **3D** reconstruction quality*

resulted from overlap/sidelap changes for Ideal, Excellent, Good, Moderate, and Poor conditions. (a) and (b) are the minimum, mean, and maximum values of horizontal and overall errors of **3D** reconstruction. (c) and (d) are the normalized values of these errors relative to the minimum values

Furthermore, in all five modes, increasing both overlap and sidelap simultaneously leads to a decrease in 3D reconstruction error. However, a more detailed comparison can be made by examining the diagrams in Figure 9.

Moreover, across all five modes, the impact of sidelap on improving the accuracy of overall 3D reconstruction is greater than that of overlap. This becomes apparent as the difference between overlap and sidelap increases. For example, in the Good mode diagram (numerical values not directly visible), the first case of px=95, py=30 and the second case of px=30, py=95 exhibit the largest difference in overall 3D reconstruction error (RMSExyz), with the first error (0.76 GSD) being, on average, 15% higher than the second error (0.66 GSD). However, it is not recommended to prioritize increasing sidelap over overlap to enhance accuracy, as it would incur higher costs and imaging duration. Conversely, symmetrical changes in overlap and sidelap have nearly identical effects on the horizontal error of 3D reconstruction. Additionally, in the five modes, it can be concluded that the majority of 3D reconstruction errors (RMSExyz) occur when one overlap is between 50% and 80% and the other is between 30% and 45%. Therefore, if one overlap is set below 50%, the other should be adjusted to 85% to 95%, or both overlaps should exceed 50% to prevent an increase in reconstruction error.

Furthermore, according to the diagrams in Figure 8, for the five modes, it is apparent that when overlaps are below 60%, increasing sidelap does not necessarily reduce the 3D reconstruction error (RMSExyz). Similarly, increasing overlap does not necessarily decrease the error when sidelap is below 60%. This irregular behavior of errors can be attributed to the diminished geometric strength of the network. Another contributing factor is the increased significance of the overall base of overlapping images relative to the value of individual overlapping images.

Lastly, based on Figure 9, when the sum of overlap and sidelap is equivalent, an approximately 50% increase in the maximum horizontal and overall error of 3D reconstruction occurs due to a decrease in the number of space-intersected rays. However, this trend does not hold when the total overlaps are equal to or less than 120%. In such cases, the network's low strength results in a maximum reduction of the overall 3D reconstruction error by 25%. Therefore, when total overlap and sidelap exceed 120%, it is advisable to maximize their difference, whereas for cases with total overlap and sidelap below 120%, it is preferable to keep overlap and sidelap values as close to each other as possible.

3.2. Flight altitude impact on 3D reconstruction accuracy

To conduct the test, the flight altitude is adjusted based on the values specified in the change column of Table II.
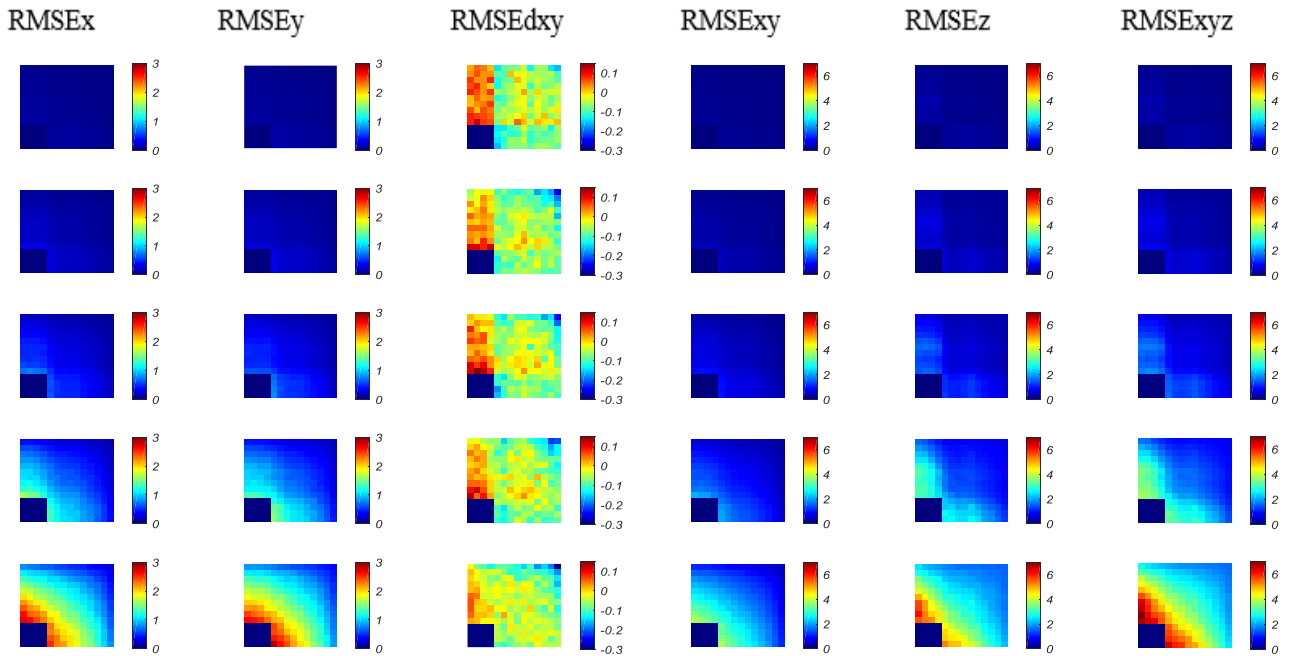
Subsequently, the 3D reconstruction simulation is repeated. The outcomes of this test are illustrated in Figure 10.

As depicted in Figure 10, the 3D reconstruction's horizontal and vertical errors exhibit a linear increase as the flight altitude is raised. Therefore, altering the flight altitude from half to twice the standard value leads to a corresponding change in the horizontal and vertical errors of the 3D reconstruction, ranging from half to double the initial error. In other words, unlike the stereo mode where the vertical error of the 3D reconstruction is influenced by twice the flight altitude, the vertical error, similar to the horizontal error, follows the flight altitude during multiple imaging. In this test, the vertical error is represented by the red color, while the horizontal error is denoted by the blue color.
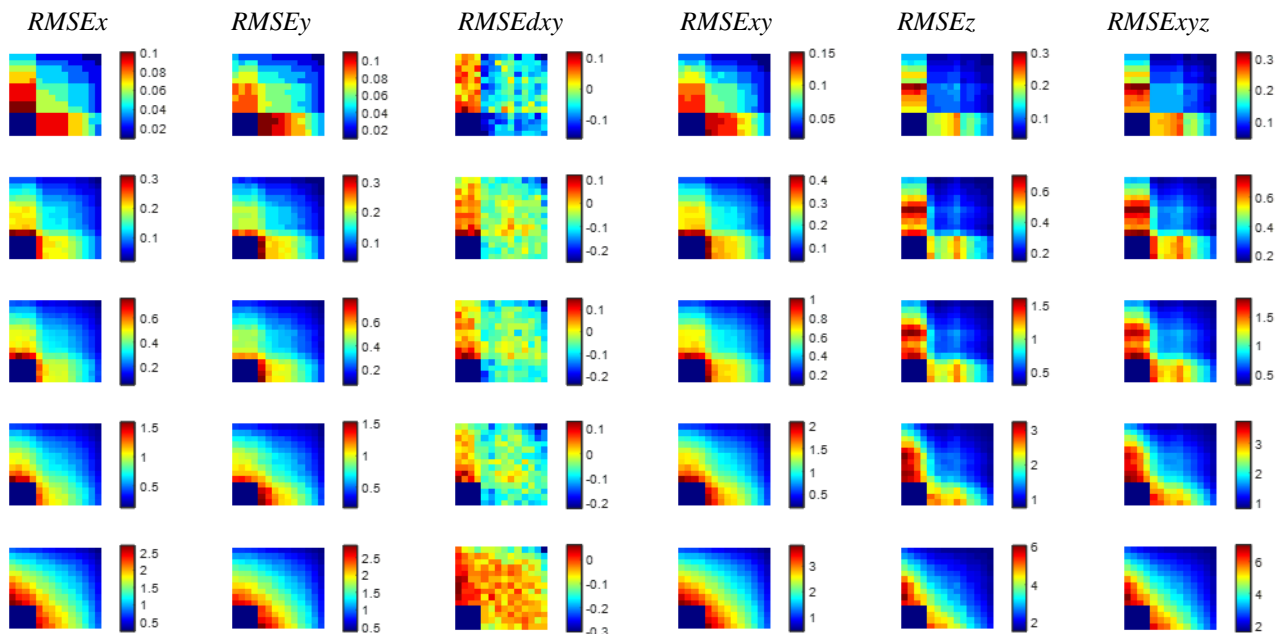
3.3. Changing image overlap and flight altitude to preserve 3D reconstruction quality

During this test, modifications were made to the flight altitude and overlap-sidelap values based on the variations outlined in Table 2. Subsequently, a 3D reconstruction simulation was performed. The outcomes of this test are displayed in Figure 11.

As depicted in Figure 11, the 3D reconstruction errors, denoted as e, exhibit an almost linear relationship with respect to the two parameters that were tested, x1 and x2. Consequently, it is possible to fit a regression plane equation to the error values using Equation (13).

a: similar color scales for each column to figures can be comparable in different modes

b: different color scales for each case in order to clearly illustrate the error behaviour

Figure 8. 3D reconstruction by changing the overlap (horizontal 30:5:95 percent) and sidelap (vertical 30:5:95 percent) from top to down for the Ideal, Excellent, Good, Moderate, and Poor modes and from left to right for RMSEx, RMSEy, RMSEdxy, RMSExy, RMSEz, and RMSExyz. Colorbars in Figure 8a have similar scales for each column, but in Figure 8b, they have local scales for each case.
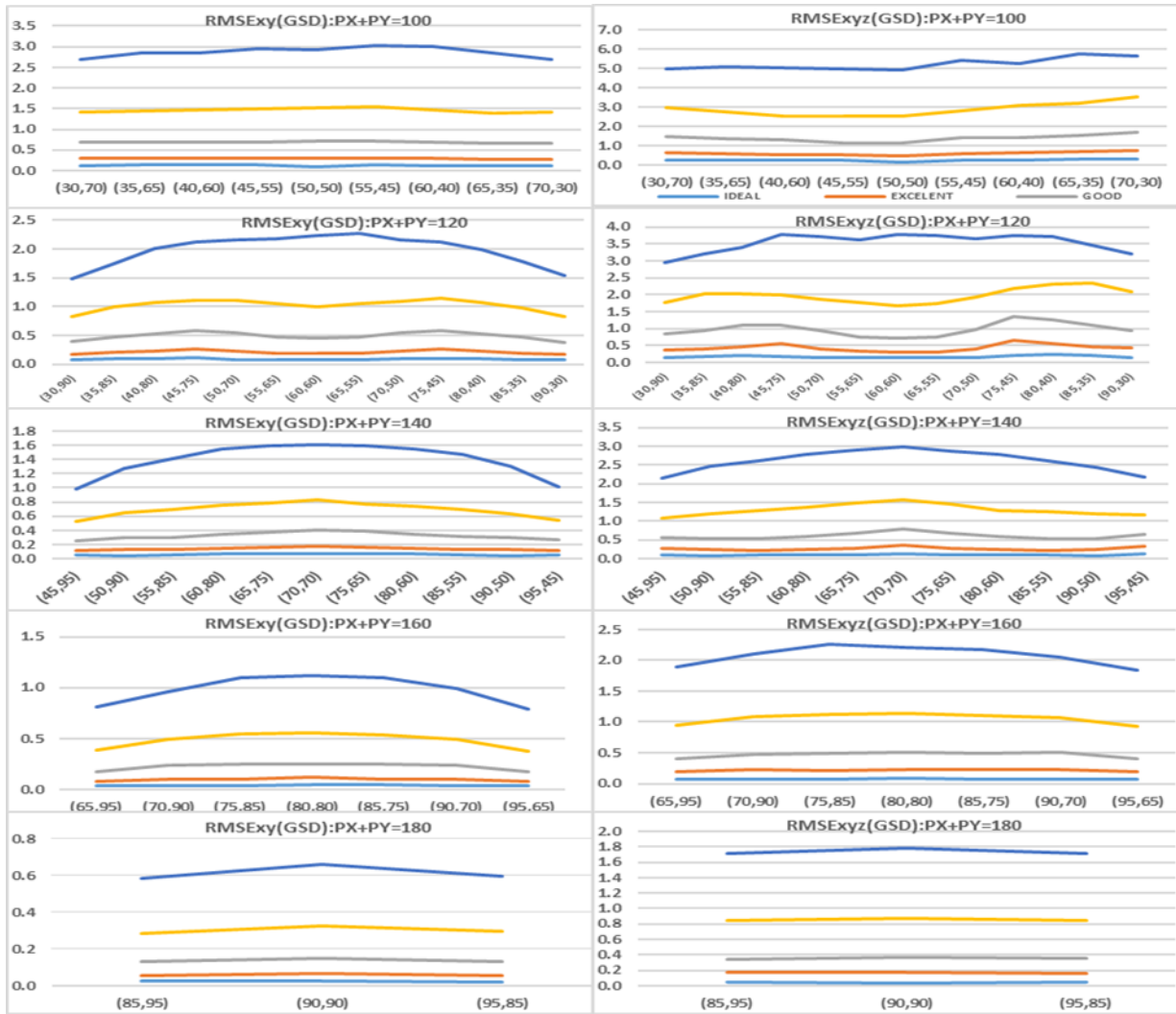
*Figure **9**. Changes of 3D reconstruction horizontal and overall error (vertical axis GSD) for constant px+py (horizontal axis %) in the five modes (the index of different colors is shown in the top-right diagram).*
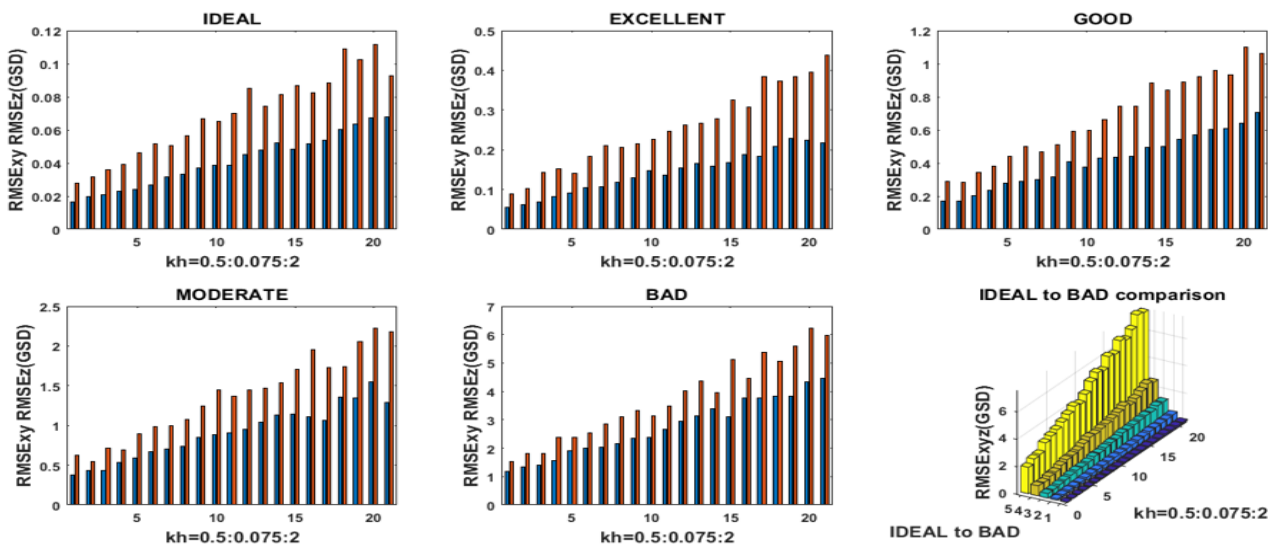

Figure 10. Results of the test of the impact of flight altitude on the accuracy of 3D reconstruction (GSD is the value appropriate for kh=1)
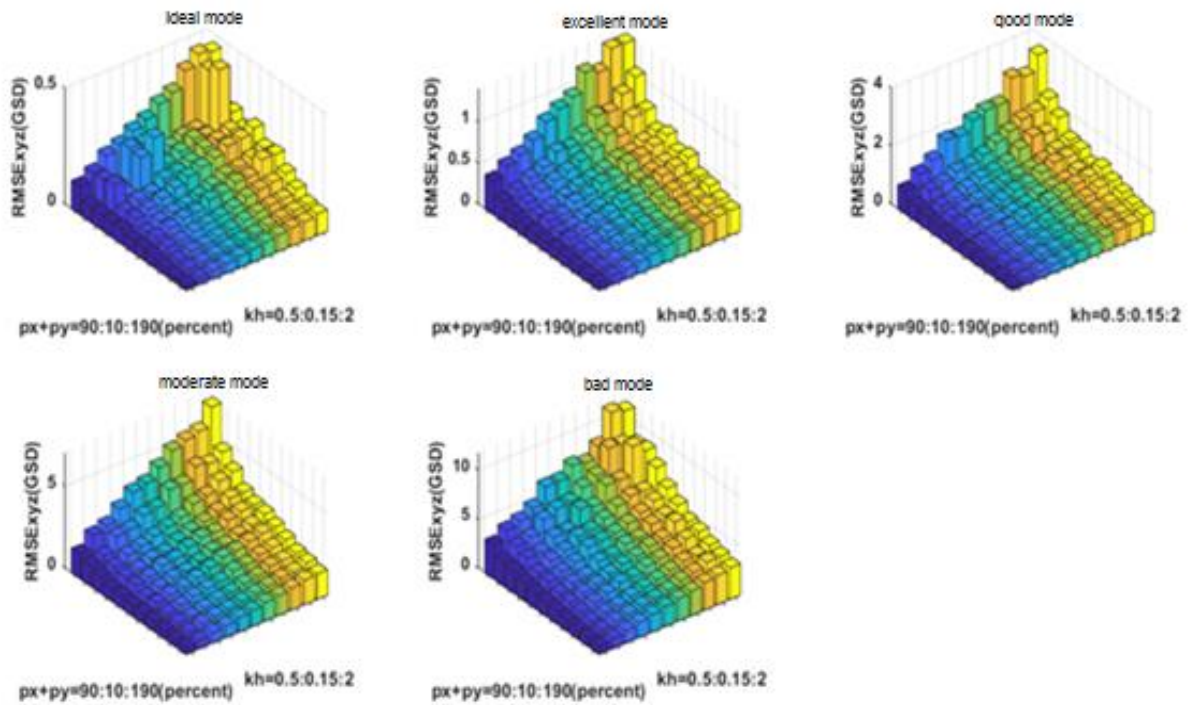
Figure 11. Impact of simultaneous change of flight altitude and image overlapping on the accuracy of 3D reconstruction in the five modes

To understand how the parameter x1 changes with the value of dx1 and how the parameter x2 should be adjusted to maintain the 3D reconstruction error, we introduce new variables: $X'1 = x1 + dx1$ and $X'2 = x2 + dx2$. By substituting these definitions into Equation (13), we can derive Equation (14). It is important to note that preserving the quality of the 3D reconstruction requires equality between Equations (13) and (14). Based on the relationship between the two parameters p1 and p2, as outlined in Equation (16), we can obtain Equation (15).

$$e = p1.x1 + p2.x2 + p3 \tag{13}$$

$$e = p1.(x1 + dx1) + p2.(x2 + dx2) + p3 \tag{14}$$

$$p1.dx1 + p2.dx2 = 0$$

$$dx2 = -\frac{p1}{p2}.dx1$$

(15)

(16)

To predict the necessary adjustment in parameter x2, given a change in x1, in order to maintain the accuracy of the 3D reconstruction, we calculate the coefficient $k = -p1/p2$. This coefficient allows us to determine both the magnitude and direction of the change in x2 (dx2) as $dx2 = k*dx1$. To calculate the parameters p1 and p2, equations need to be established based on Equation (13) using the values of x1, x2, and the corresponding reconstruction error resulting from their simultaneous change. By constructing the coefficient matrix of observations and unknown values,

p1 and p2 can be calculated through the method of least squares of errors. The results of this analysis are presented in Table 3, which will be further analyzed and investigated in the subsequent section.

Table 3. Coefficients of 3D reconstruction accuracy preservation by changing the flight altitude after changing the overlap and sidelap sum.

Quality Measure	Flight altitude compensation coefficients after changing 10% sum of image overlap and sidelap				
Mode	Ideal	Excellent	Good	Moderate	Poor
RMSExy	0.021	0.022	0.021	0.021	0.020
RMSEz	0.016	0.012	0.013	0.011	0.013
RMSExyz	0.018	0.014	0.015	0.014	0.015

Based on the findings presented in Table 3, we can draw the conclusion that in order to maintain the horizontal 3D reconstruction accuracy (RMSExy), if the total overlap and sidelap of images are decreased or increased by 10%, the flight altitude should be adjusted accordingly. Specifically, in all five modes, the flight altitude needs to be decreased or increased by 20% of the standard flight altitude. This adjustment ensures the preservation of the horizontal 3D reconstruction accuracy.

3.4. Comparing different cameras and lens FOVs on 3D reconstruction simulation

The objective of this section is to examine the impact of changes in camera lens field of view (FOV) on the simulation analysis. To address this question, we have expanded our testing to include two additional practical camera/UAV systems: the DJI Phantom 4 Pro and a fixed-wing UAV equipped with the Sony α6000. These systems have been included alongside the DJI Phantom 3 UAV system in Table 4, allowing us to provide a partial answer to the question at hand.

Table 4. UAV/Camera Systems characteristics utilized for simulation

UAV System	Lens Focal Length (mm)	Sensor Size (pixels)	Pixel Size (µm)	FOV (Degrees)
DJI-Phantom3	3.5891	4000*3000	1.5619	95
DJI-Phantom4pro	9.1128	5472*3078	2.5269	82
Fix-wing Sony α6000	25.9480	7952*5304	4.5265	80

3.4.1 Comparing different cameras and lens FOVs on 3D

We have successfully completed a total of 900 tests for the two additional UAV/Camera systems. After analyzing the results, we have observed that they exhibit a high degree of similarity and compatibility, with variations ranging from 10 to 20 percent, as depicted in Figure 12. This indicates that our simulation results are highly reliable and can be effectively generalized for lens FOV values ranging from 80 to 95 degrees.

Figure 12. Average RMSExyz (unit GSD) of 3D reconstruction for simulation with different UAV/Camera systems

4. Conclusion

In the present study, the simulation method was employed to address real-world challenges related to the analysis of flight altitude and image overlap/sidelap. However, certain factors such as flight speed and achieving a balance between the limitations of sensor firing speed due to hardware constraints and image blurring were not taken into account. The key findings of this research can be summarized as follows: The modification of overlap and sidelap can enhance the horizontal (RMSExy) and overall (RMSExyz) error of 3D reconstruction by up to 10 and 5 times, respectively. Furthermore, the study revealed that the heterogeneity of errors along the overlap and sidelap ranges

from 15% to 30% of the horizontal errors, with greater heterogeneity observed when both overlap and sidelap exceed 80% or fall below 55%.

Furthermore, this study indicates that for imaging with a total overlap and sidelap of more (or less) than 120%, it is better to consider the values of overlaps far from one another as much as possible. In other words, when the sum of the overlap and sidelap is more than 120%, a higher overlap and a lower sidelap would achieve a higher 3D reconstruction accuracy. However, when the sum is less than 120%, it is better to set overlap and sidelap relatively close to each other.

Another practical result of this study based on our experiments is that if one overlaps is chosen to be below 50%, the other overlap must be 85% to 95%, or both overlaps must be above 50% so that the 3D reconstruction quality will not be lost. Although by the simultaneous increment of both overlaps and sidelap, the 3D reconstruction quality will always increase, in the case of overlaps and sidelap below 60%, the increment of overlapping in one direction will not necessarily improve the reconstruction quality. Also, it could be stated that the increment of the sidelap improves the 3D reconstruction quality more effectively than the overlap, while both overlap/ and sidelap have the same impact on the improvement of horizontal quality.

Another result of this study based on our experiments is that the horizontal and vertical error will increase by increasing flight altitude.

Another significant result is that by decreasing the sum of overlap/sidelap by 10%, the flight altitude must be decreased by 20% to compensate for the reduction of horizontal 3D reconstruction accuracy. To preserve the horizontal accuracy, if the flight altitude increases by 20%, the sum of the overlap and sidelap must also be increased by 10%.

In the end, it should be noted that all these simulation outcomes are based on our special experiments and need additional real-world cross-checks to be considered as new knowledge and rule in UAV photogrammetry. In addition, although the above result of the first phase of simulation analysis is precious, the second and third phases give us more realistic and more complete results at the cost of more complexity.

Our future research will concentrate on two subjects. Since the outcomes of this research are derived from a simulation process, we plan to examine them practically in our future research. In addition, to improve the simulation process, we will develop it to reconstruct a group of 3D hypothetical points simultaneously instead of a single point.

References

Barry, P., Coakley, R. (2013). ACCURACY OF UAV PHOTOGRAMMETRY COMPARED WITH NETWORK RTK GPS. Arch Int la Fotogram remoto. http://www.uav.ie/PDF/Accuracy_UAV_compare_RTK_GPS.pdf.

Cryderman, C., Mah, S.B. Shufletoski A. (2014). EVALUATION OF UAV PHOTOGRAMMETRIC ACCURACY FOR MAPPING AND EARTHWORKS COMPUTATIONS. G E O M A T I CA Eval, 68(4), 309-317.

Christoph, H., Candela, P. (2014). Research Collection. Brisk Bin Robust Invariant Scalable Keypoints,0-2. https://doi.org/10.3929/ethz-a-010025751.

Doringer, B. (2018). The beginning of the MONT CARLO METHOD. Faceless Re-inventing Priv through Subvers Media Strateg, 6-16. doi:10.1177/004057368203900302

Doug, H. (2007). How to Measure Anything: Finding the Value of Intangibles in Business.; John Wiley & Sons; pp. 23.

Erfanzadeh, A., saadatseresht, M. (2021). The Simulation Analysis of the Effect of Imaging Sidelap/Overlap on the Quality of 3D Reconstruction in UAV Photogrammetry and Determination of their Optimal Values, Geospatial Information Technology, 9(1) (2021) 105-124

HENRI, E. (2009). UAV Photogrammetry. Doctoral Thesis, University of Technology Dresden, Zurich, Germany. https://doi.org/10.3929/ethz-a-005939264.

Hastedt, H. (2004). Monte-carlo-simulation in close-range photogrammetry. ISPRS. 7, 34. https://www.researchgate.net/publication/2950540

Kim, H., Robert, C.P., Casella, G. (2000). Monte Carlo Statistical Methods. Technometrics, 42(4):430. doi:10.2307/1270959

Leitão, J.P., Vitry MM, D.e., Scheidegger, A., Rieckermann, J. (2015). Assessing the quality of Digital Elevation Models obtained from mini-Unmanned Aerial Vehicles for overland flow modelling in urban areas. Hydrol Earth Syst Sci Discuss, 12(6):5629-5670. doi:10.5194/hessd-12-5629-2015

Mesas-Carrascosa, F.J., Clavero Rumbao, I., Torres-Sánchez, J., García-Ferrer, A., Peña, J.M., López Granados, F. (2017) . Accurate ortho-mosaicked six-band multispectral UAV images as affected by mission planning for precision agriculture proposes. Int J Remote Sens,38(8-10):2161-2176. doi:10.1080/01431161.2016.124931

Mesas-Carrascosa, F.J., Torres-Sánchez, J., Clavero-Rumbao, I. (2015). Assessing optimal flight parameters for generating accurate multispectral orthomosaicks by uav to support site-specific crop management. Remote Sens, 7(10):12793-12814. doi:10.3390/rs71012793

Mesas-Carrascosa, F.J., García MDN, D.e., Larriva, J.E.M., García-Ferrer, A. (2016). An analysis of the influence of flight parameters in the generation of unmanned aerial vehicle (UAV) orthomosaicks to survey archaeological areas. Sensors (Switzerland), 16(11). doi:10.3390/s16111838

Palisade. Available online: https://www.palisade.com/risk/monte_carlo_simulation.asp.

Remondino, F., Barazzetti, L., Nex F, Scaioni M., Sarazzi, D. (2012). Uav Photogrammetry for Mapping and 3D Modeling – Current Status and Future Perspectives. Int Arch Photogramm Remote Sens Spat Inf Sci, XXXVIII-1/(September):25-31. doi:10.5194/isprsarchives-xxxviii-1-c22-25-2011

Rock, G., Ries, J.B., Udelhoven, T. (2012). Sensitivity Analysis of Uav-Photogrammetry for Creating Digital Elevation Models (Dem). Int Arch Photogramm Remote Sens Spat Inf Sci, XXXVIII-1/(September 2016):69-73. doi:10.5194/isprsarchives-xxxviii-1-c22-69-2011

Radoslaw Jan, R. (2017). Accuracy analysis of products obtained from UAV-borne photogrammetry influenced by various flight parameters. master thesis, University of Science and Technology, Norwegian.

SENKAL, E., KAPLAN, G., AVDAN, U. (2021). Accuracy Assessment of Digital Surface Models from Unmanned Aerial Vehicles' Imagery on Archaeological Sites. Int J Eng Geosci,6(2):81-89. doi:10.26833/ijeg.696001

Shahbazi. M., Sohn, G., Théau, J., Menard, P. (2015). Development and evaluation of a UAV-photogrammetry system for precise 3D environmental modeling. Sensors (Switzerland), 15(11):27493-27524. doi:10.3390/s151127493

Zhang, Y., Xiong, J., Hao, L. (2011). Photogrammetric processing of low-altitude images acquired by unpiloted aerial vehicles. Photogramm Rec, 26(134):190-211. doi:10.1111/j.1477-9730. 2011. 00641.x